Cement and Concrete Composites 145 (2024) 105324

Contents lists available at ScienceDirect

Cement and Concrete Composites

journal homepage: www.elsevier.com/locate/cemconcomp

Biogenic acid resistance of calcium sulfoaluminate cement: Revelations from a field study

Tom Damion, Piyush Chaunsali *

Department of Civil Engineering, Indian Institute of Technology Madras, Chennai, India

ARTICLE INFO

Keywords:
Sulfuric acid
Calcium sulfoaluminate cement
Sewer
Thiobacilli
Biogenic acid attack

ABSTRACT

Biogenic acid attack of concrete is prevalent in sewers, posing a serious durability concern and financial burden. There are very limited number of field studies on durability of concrete under biogenic acid attack. Field study poses challenges with respect to the variation in climatic conditions and limited accessibility in sewers. Such a biogenic acid attack study in Indian conditions has not been performed. In this study, the biogenic acid resistance of Portland cement (PC) and calcium sulfoaluminate (CSA) cement-based binders under an in-situ sewer exposure is reported. The results show that the CSA-based binder used in this study outperformed PC in the biogenic acid resistance. The superior performance of CSA-based binder could be attributed to its acid neutralisation capacity offered by the aluminum hydroxide phase and bactericidal properties. For the first time, the bacteriostatic effect of CSA cement was demonstrated by analyzing the field exposed specimens.

1. Introduction

Acid attack of cement-based composites is a common deterioration problem in the structures exposed to acidic environments. Severe deterioration of masonry mortar and the lining material, near the roof and walls of the structure, was observed in an outfall sewer after two years of construction in Los Angeles in the year 1895 [1]. It was found that the hydrogen sulfide (H_2S) which oxidized into sulfuric acid (H_2SO_4) was responsible for this damage. The damaged cement paste was identified with the formation of silica and gypsum. Swelling in the mortar was thus attributed to expansive gypsum [1]. Later, many similar acid-attack cases of sewer structures were reported in Australia, Cairo, and Cape Town in the first half of the twentieth century. In all these cases, the H_2S-to-H_2SO_4 conversion was viewed as the chemical process leading to deterioration. It was not until 1945 that C. D. Parker emphasized the involvement of bacteria similar to Thiobacillus thiooxidans in the damage process [2,3]. Sulfate-reducing bacteria were found to be responsible for H_2S formation [4]. Hence, this bacteria-involved acid attack came to be known as biogenic acid attack.

Biogenic acid attack of cement-based composites involves three stages [5,6]. Various stages involved in it can be visualised through the change in surface pH. Fig. 1 explains the three stages in the biogenic acid attack. The bacteria cannot survive in a high pH environment such as in concrete. But the carbonation or the exposure to H_2S or the attack of other acids (acetic acid, oxalic acid, and glucuronic acid) secreted by fungi reduces the surface pH of concrete to 9–10. This marks the end of Stage 1 of the biogenic acid attack, and it takes around 1–8 weeks for its completion. When the pH is reduced to 9, thiobacillus bacteria can colonise with enough moisture, nutrients, and available oxygen [7]. *Thiobacillus thioparus* (neutrophilic) can survive in pH of 6–10 and oxidizes H_2S to products having various sulfur states such as thiosulfate, tetrathionate, and elemental sulfur and ultimately to sulfuric acid, which further reduces pH to 4–5 [8]. This indicates Stage 2 of the attack and a biofilm is attached to concrete surface. Acidophilic bacteria such as *Acidithiobacillus thiooxidans* thrive in pH less than 4 and oxidizes H_2S directly to sulfuric acid, triggering the onset of Stage 3 [9]. The time for initial pH reduction depends on the sewer environmental characteristics such as H_2S and CO_2 concentration. On increasing the temperature (e.g., 16 °C–30 °C) and the relative humidity, the acidification and neutralisation of concrete surface are accelerated [10].

Stage 3 of microbial induced corrosion can be simulated by utilizing biogenic sulfuric acid or by chemical acid attack tests [11]. In contrast to the biogenic acid attack test, the chemical acid attack test does not provide any information regarding binder's bacteriostatic effect. The bacteriostatic effect refers to the ability of a binder to stop the growth or metabolic activity of bacteria. This is significant and must be measured in an aggressive environment [12]. For example, biogenic acid resistance of calcium aluminate cement (CAC) can be attributed to the

* Corresponding author.
E-mail address: pchaunsali@iitm.ac.in (P. Chaunsali).

https://doi.org/10.1016/j.cemconcomp.2023.105324
Received 16 May 2023; Received in revised form 16 September 2023; Accepted 9 October 2023
Available online 10 October 2023

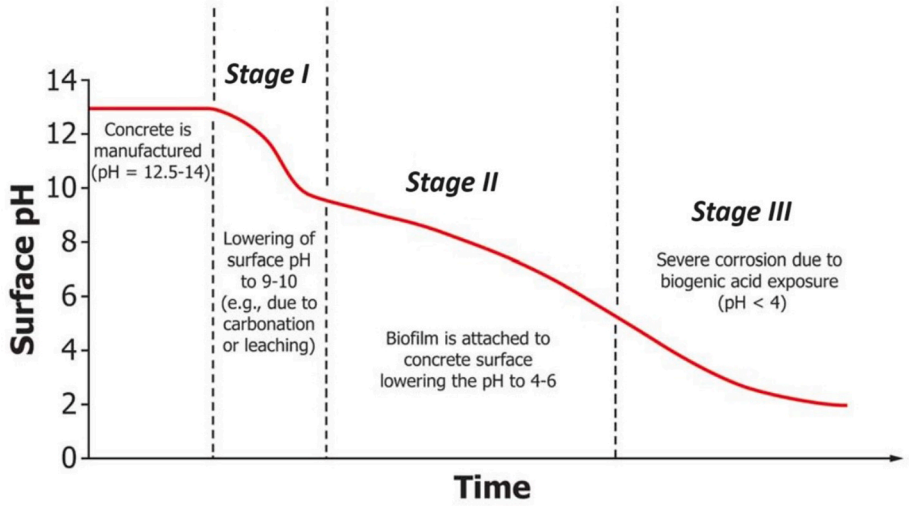

Fig. 1. The three stages of biogenic acid attack [9].

Table 1
Oxide composition.

Binders	SiO_2	CaO	Al_2O_3	SO_3	Fe_2O_3	MgO	K_2O	TiO_2	SrO	Na_2O	LOI*
CSA (LY)	3.6	56.9	6.3	24.6	0.8	1.7	0.3	0.4	0.2	0.0	5.3
CSA (HY)	14.0	39.8	20.9	14.5	3.6	2.8	0.5	1.1	0.1	0.2	1.8
PC	18.9	63.3	5.2	2.7	5.7	0.9	0.6	0.5	0.0	0.0	2.2

LOI*: Loss on ignition.

bacteriostatic effect of CAC [13]. Hence, the acid resistance has to be evaluated through the experiments performed in a biogenic acid environment [14]. The biogenic acid attack can be simulated by culturing bacteria in the laboratory and exposing the specimens to it as reported in Refs. [11,15–19]. The simulation tests, depending on the methodology, may sometimes become advanced state of chemical acid immersion test without focusing on Stage 1 and Stage 2 of biogenic acid attack [7,20]. For a better understanding of biogenic acid attack, specimens can be suspended in live sewer environment [21,22]. However, the sewer conditions vary with respect to gaseous concentration, temperature, relative humidity, wastewater level, wastewater characteristics, turbulence, and bacterial diversity [5,23]. Further, in-situ sewer test can take a long time period for evaluating the relative performance of binders [24], as the deterioration rate starts from 0.6 mm/year [25] depending on the sewer characteristics. Very limited field study data are available from structures other than circular sewers.

For applications in sewer environment, the approach of making binder antimicrobial by using benzoate was reported in Refs. [26,27]. Various antimicrobial concrete mix compositions involving the application of nanotechnology have been summarized in Ref. [28]. CAC has been found to be effective against biogenic acid attack by stifling *Thiobacillus* metabolism and preventing acid generation [13]. Increased release of aluminium (Al) ion provides the bacteriostatic effect [29].The bacteriostatic effect is based on the reaction of some positively charged metal ions with the negatively charged cell wall of the bacteria. This leads to the formation of complex compounds within bacterial cell membrane. This inhibits the activity of life essential enzymes and can even affect the osmotic stability of the cells [30]. Aluminium has been suggested to have bactericidal property [31,32]; but it has not been verified [33,34]. In addition to that, leaching of calcium ions leads to aluminum-rich layer, which acts as a protective layer [35]. CAC reported lower mass loss than PC after 150 days in simulation chamber [36]. Though CAC has good resistance in sewer environment, high cost and undesirable conversion reaction are its main drawbacks. Among alternative binders for such application, calcium sulfoaluminate (CSA) cement, which is a low CO_2 binder, has useful characteristics such as rapid hardening and shrinkage-compensation. Moreover, this binder differs significantly from PC with respect to phase assemblage and alkalinity of pore solution. The total global sewer network length was approximated to be greater than ten times the diameter of the earth [25]. Hence, large amount of cement is required for these structures. Sustainable cements are required to reduce the carbon footprint associated with this huge construction. The higher kiln temperature of CAC [37] makes it less sustainable in terms of energy requirement as compared to CSA cement which can be manufactured at ~1250 °C [38].

Hydrated CSA cement, similar to hydrated CAC, contains aluminum hydroxide and can be a potential candidate for sewer structures. In an in-situ sewer exposure experiment reported by Ref. [39], it was found that CSA cement outperformed sulfate resisting Portland cement. Hence, a double-edged benefit with regard to achieving durability and sustainability is possible through the use of CSA cement. For that, durability of hydrated CSA cement against acid attack needs to be evaluated. In this study, the suitability of CSA cement in sewer structures is evaluated by monitoring its biogenic acid resistance in a real sewer environment exposure for one year. The mechanism of biogenic acid attack of CSA cement is also examined with respect to its similarity to titrimetric results.

2. Materials and methods

Portland Cement (PC) of grade 53 as per IS 269: 2015, commercially available CSA cement (CSA(HY)), and CSA admixture (CSA(LY)) were used in this research. The oxide compositions of the raw materials are shown in Table 1.

CSA (LY) was lime-rich CSA-based expansive admixture for PC. However, CSA (HY) was a rapid hardening non-expansive binder and used as a sole binder. CSA (LY) was blended with PC at a dosage of 10 % (by weight) which offered maximum Oxygen Permeability Index (OPI) value and hence maximum impermeability. PC, CSA (HY), and CSA (LY) binders had specific gravity of 3.15, 2.86, and 2.67, respectively. The d_{50}

Table 2
Phase composition (%) of raw materials.

Phases/Binder	CSA (LY)	CSA (HY)	PC
Ye'elimite	11.1	35.5	0.0
Anhydrite	47.3	15.5	0.0
Gypsum/Bassanite	0.0	1.5	3.1
Lime	20.1	3.9	0.0
Dicalcium silicate	5.3	28.7	32.8
Dolomite	11.6	7.6	0.0
Portlandite	1.3	0.0	0.0
Brownmillerite	2.4	3.5	7.2
Mayenite	0.9	2.1	0.0
Quartz	0.0	1.7	0.0
Tricalcium silicate	0.0	0.0	47.4
Tricalcium aluminate	0.0	0.0	5.5
Calcite	0.0	0.0	3.9

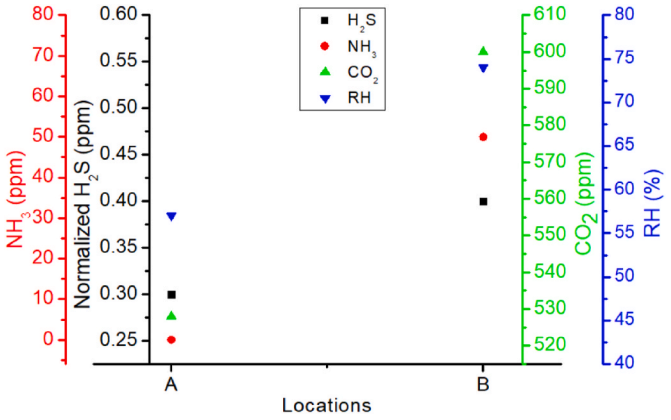

Fig. 2. Characteristics of the sewer locations A and B at IITM campus – concentrations of H_2S, NH_3, CO_2 and relative humidity (RH).

particle size values were 11.2 μm, 7 μm, and 9.5 μm for PC, CSA(LY), and CSA(HY) binders. The phase compositions of the raw binders (100 % crystalline) determined by XRD analysis are shown in Table 2.

The standard sand as per IS 650:1991 was used for the preparation of mortar. All three grades of sand with particle size distribution from 1000 to 2000 μm, 500–1000 μm, and 90–500 μm were mixed together in equal proportions [40].

2.1. Field study

As far as biogenic acid attack or sewer corrosion is considered, it is important to identify a location based on concentrations of hydrogen sulfide (H_2S), ammonia (NH_3), carbon dioxide (CO_2) and relative humidity (RH). These characteristics vary depending on the wastewater characteristics, flow velocity, and hydraulic retention times. The suitable locations were shortlisted based on the level of corrosion and the favorable conditions leading to it. The measured sewer characteristics for two locations are plotted in Fig. 2.

The concentration of H_2S is underestimated as its density is 1.36 kg/m^3 and will be concentrated at bottom level of sewer locations with less availability at the point of measurement near ground level. The measurement was performed immediately after opening the manhole cover to reduce the H_2S escape in the process. It must be noted that the H_2S flux in a closed environment would be high and increasing due to continuous accumulation. Ammonia (NH_3) has a density of 0.73 kg/m^3 and could be easily detected: in some cases crossing the maximum capacity of the meter (50 ppm). Carbon dioxide has a density of 1.98 kg/m^3 at room temperature. The CO_2 concentrations at the locations were high, indicating the possible accelerated carbonation or Stage 1 of biogenic acid attack. The relative humidity is contributed by the moisture in air. When the relative humidity is high, the deterioration of suspended specimens above wastewater level will also increase. The relative humidity provides water film for the microbial growth in the crown region or on the suspended specimen surface [41]. In order to showcase the seasonal variation, the H_2S concentration was measured

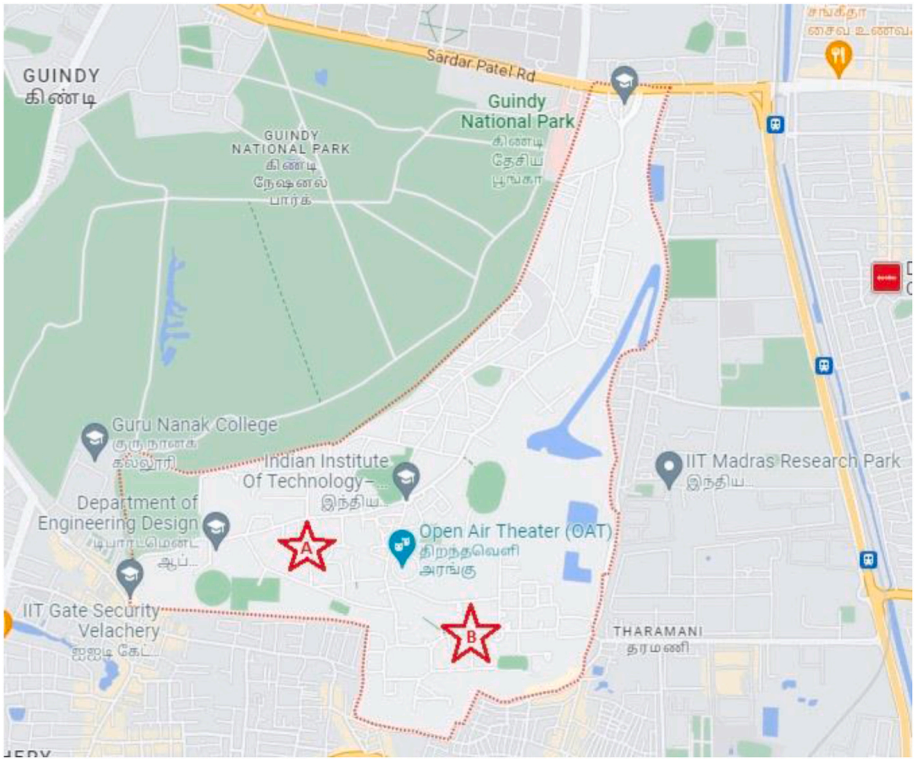

Fig. 3. The locations *(A and B)* for in-situ sewer exposure (Source: Google Maps).

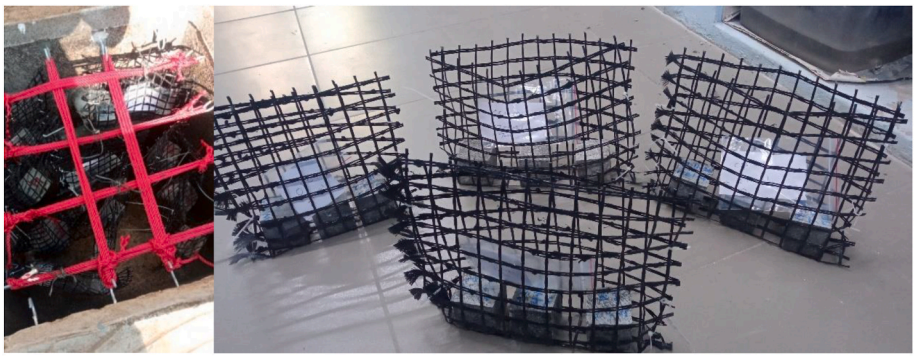

(a) (b)

Fig. 4. (a) Suspension of specimens at *Location A*, and (b) Specimens inside basket with label in Ziplocs

Table 3
Mixture proportions (by wt. %).

Terminology	Binder			w/b	Sand	Location
	PC	CSA (LY)	CSA (HY)			
PC paste	100 %			0.4	0	Location B
PC-CSA(LY) paste	90 %	10 %		0.4	0	Location B
CSA(HY) paste			100 %	0.4	0	Location B
PC mortar	100 %			0.4	3 times binder	Location A
PC-CSA(LY) mortar	90 %	10 %		0.4	3 times binder	Location A
CSA(HY) mortar			100 %	0.45	3 times binder	Location A

after the first Monsoon rain in Chennai during June 2022. It was observed that there was a slight reduction in concentration level of H_2S after the rain. A feasibility study was conducted before finalising the locations. Further, considering the variation of sewer characteristics across location and time, sewers were finalized based on their biogenic acid attack history. The locations (A and B) used for the in-situ biogenic acid attack study are shown in Fig. 3. The locations are part of campuswide sewer network of IIT Madras (Chennai, India).

Mortars and pastes were used in the study. The mixing was performed according to ASTM C305: 2020 in a front-mounted planetary Hobart mixer. CSA(LY) mix was dry-mixed (with 90 % wt. of PC) for 5 min before adding water to ensure homogeneity of the mix. The specimens were cured for 28 days in a mist room.

Mortar (1 part binder: 3 parts sand) cubes of size 50 × 50 × 50 mm were suspended in triplicate inside a basket at *Location A (12.9899 N, 80.2303 E)* as shown in Fig. 4. The binders included PC, PC-CSA(LY) blend, and CSA(HY) cement. The mix proportions are shown in Table 3. The water-to-cement ratio (w/c) for PC-dominated binders was 0.4 and CSA(HY) had w/c of 0.45 to obtain consistent mix without the addition of superplasticiser. The flow was measured immediately after mixing. The flow table test was performed as per ASTM C1437–2007. The flow was measured as the resultant increment (%) in the average base diameter of mortar frustum with respect to the initial diameter [42]. Compressive strength was determined after 28-day of curing in a mist room. The loading rate for the compressive strength test was 900 N/s.

The prismatic paste specimens of size 40 × 40 × 160 mm were suspended in triplicate inside a basket at *Location B (12.9873 N, 80.2356 E)* as shown in Fig. 5. The binders included PC, PC-CSA(LY) blend, and CSA(HY). A w/c ratio of 0.4 was used for the paste specimens.

Fig. 5. Suspension of prismatic paste specimens above water level at *Location B*.

2.2. Mass change

The mass of 28-day cured specimens was measured in the saturated surface dry condition before field exposure. After retrieving the specimens from the sewer after one year, the specimens were weighed immediately. Subsequently, the specimens were cleaned, washed, sanitised, and then weighed in saturated surface dry condition. This weight

Table 4
Flow and compressive strength of mortar specimens (*Location A*).

Mortar	w/c	Flow (%)	28-Day Compressive Strength (MPa)
PC	0.4	20	49.8 (±2.3)
PC-CSA(LY)	0.4	35	47.3 (±1.1)
CSA(HY)	0.45	25	46.5 (±2.7)

Table 5
Flexural strength of paste specimens (*Location B*).

Paste	w/c	28-Day Flexural Strength (MPa)
PC	0.4	6.6 (±0.7)
PC-CSA(LY)	0.4	4.3 (±0.4)
CSA(HY)	0.4	5.0 (±0.6)

was normalized with respect to the weight of 28-day cured specimens.

2.3. Flexural strength

Flexural strength of 40 × 40 × 160 mm prisms was determined for control prisms and prisms after one year field exposure. A span of 120 mm was marked along with centre of the specimen. Testing was performed at a loading rate of 43 N/s as per [43]. The flexural load (P) was noted and flexural strength was determined by equation below, where L is span (120 mm), b and d are cross sectional dimensions (40 mm).

$$\text{Flexural strength} = \frac{3PL}{2bd^2} \quad (1)$$

2.4. Neutralised depth

The neutralised depth was measured using phenolphthalein test. The freshly cut exposed specimens were sprayed with phenolphthalein. The altered area remained colourless and the unattacked area turned pink. The images were analysed using ImageJ software.

2.5. pH measurement

The pH of a suspension prepared by ground specimen powder was measured using the pH electrode of an automatic titrator (Metrohm 916 Ti Touch), having sensitivity of pH 0.001. The apparatus consisted of an intelligent pH electrode, temperature sensor, acid dosing unit, and a propeller stirrer. This pH was used to assess the surface and core pH of the specimen.

2.6. Turbidimetry

The biogenic acid attack resulted gypsum formation was characterised by turbidimetric technique. As explained in results section, a pinch of barium chloride was added into the suspension of ground specimen surface powder to convert sulfate into barium sulfate, inducing turbidity. The turbidity measurement enabled the quantification of gypsum. The turbidity was measured by Lutron TU-2016 Turbidity meter. It had a measuring range of 0–1000 NTU (Nephelometric Turbidity Unit) with a resolution of 1 NTU and an accuracy of ±5 % or ±5 NTU, whichever was greater.

2.7. X-ray diffraction (XRD)

Mineralogical changes were monitored using X-ray diffraction

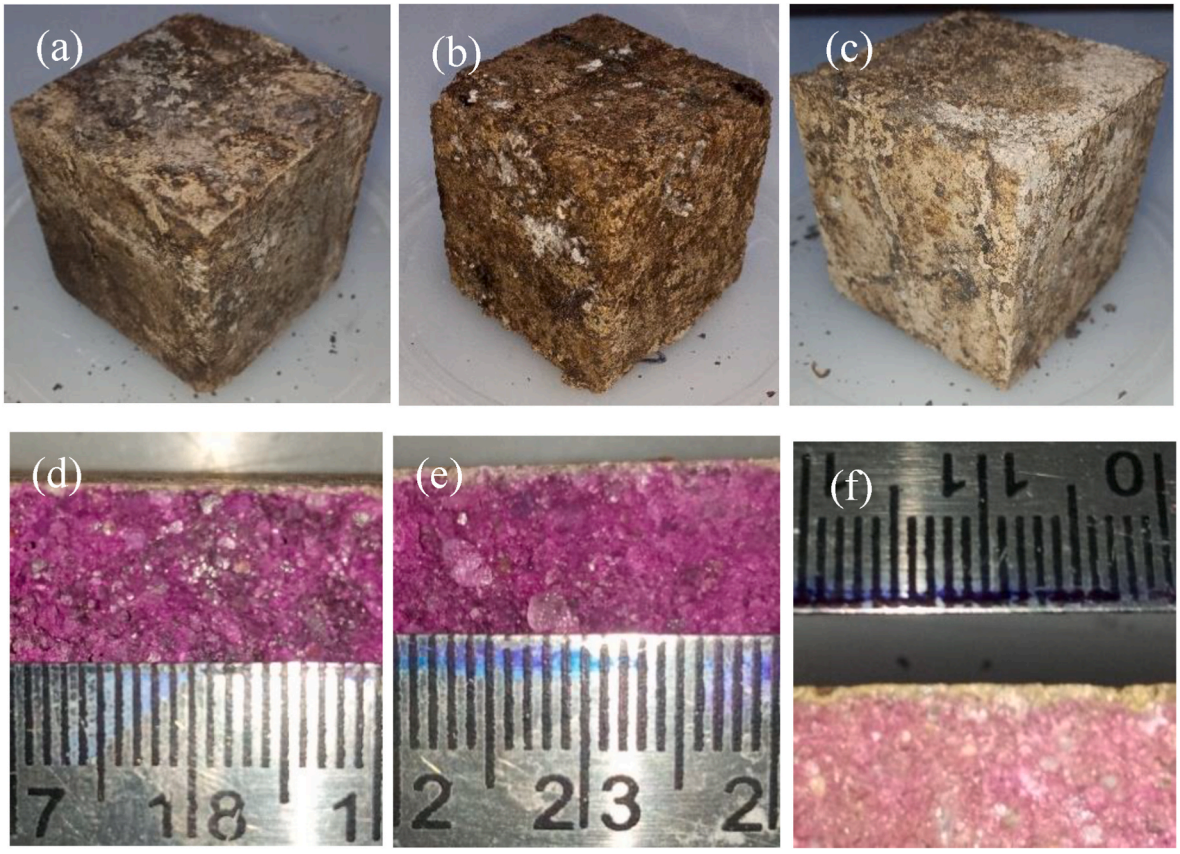

Fig. 6. Mortar specimens of: (a) PC, (b) PC-CSA(LY), and (c) CSA(HY) binders and the phenolphthalein sprayed surfaces of: (d) PC, (e) PC-CSA(LY), and (f) CSA(HY) binders from *Location A*.

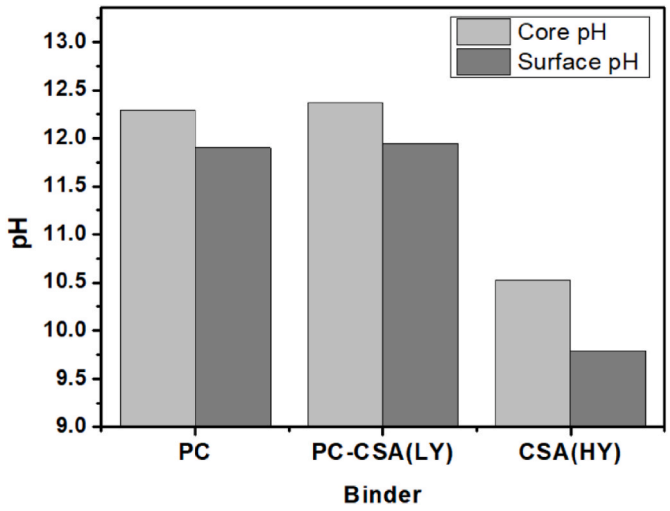

Fig. 7. Surface and core pH measured of mortar specimens from *Location A*.

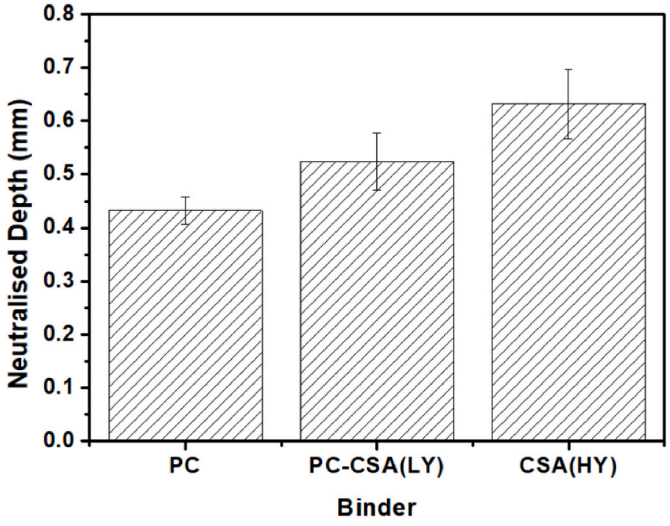

Fig. 8. Neutralisation depth assessed by phenolphthalein test of mortars from *Location A*.

(XRD). Samples were powdered and sieved through 75 μm. XRD was performed using MiniFlex Rigaku powder X-ray diffraction instrument using Cu Kα (wavelength 1.5405 Å). The tube voltage and current were 40 kV and 15 mA, respectively. The diffractogram was collected between the 2-theta range of 5°–60° with a step size of 0.02° and scanning rate of 0.2 s per step size. The diffractograms were analysed using X'Pert HighScore plus software.

2.8. Scanning electron microscopy (SEM)

Scanning electron microscopy was performed using FEI-Quanta FEG 200F equipment. Specimens were subjected to gold sputter coating before performing SEM. In case of FEI-Quanta FEG 200F equipment, dwell time was 30 μs, accelerating voltage 20 kV, beam current 1 nA, and spot size 2.5 nm.

2.9. Thermogravimetric analysis (TGA)

Thermogravimetric analysis was performed using LABSYS evo TGA from SETARAM Instrumentation. The test was carried out in the range of 30 °C–900 °C with heating rate of 15 °C/min in a nitrogen-purged environment using alumina crucibles with 5–10 mg of the sample.

3. Results

3.1. Mechanical properties of hydrated binders

The mortar specimens before exposure to the *Location A* were characterized with regard to flow (%) and 28-day compressive strength, as shown in Table 4. The 28-day cured paste specimens were exposed to the *Location B* and the flexural strength of the specimens at the time of exposure is shown in Table 5. It was necessary to maintain similar flowability, so the w/c ratio of the CSA(HY) mortar was changed to 0.45. The 28-day strengths of PC mortar and paste were found to be higher than CSA(HY) and CSA(LY) blend mixes.

3.2. Analysis of damage due to sewer exposure

The condition of the specimens was monitored during the exposure period. In the following sections, results from two locations (*Location A and Location B*) are discussed.

3.2.1. Location A (Stage 2 of biogenic acid attack)

Fig. 6 (a, b, and c) shows the alterations in the appearance of specimens after one-year of sewer exposure. These specimens were sliced after compression testing and sprayed with phenolphthalein across the cross section as shown in Fig. 6 (d, e, and f). It is evident that all specimens had a large unaffected core area fraction represented by the pink region. The surface was affected up to a small depth indicated by the non-pink colour. The intensity of pink colouration in CSA(HY) was low because of low porewater pH of these binders.

The surface and core pH were measured from the powdered samples.

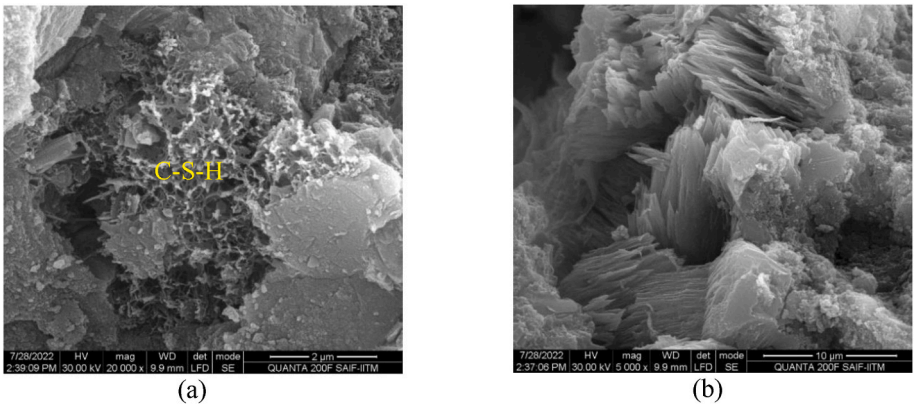

Fig. 9. SEM image of PC interface (below neutralisation depth) showing: (a) C–S–H, and (b) Columnar/flaky deposits.

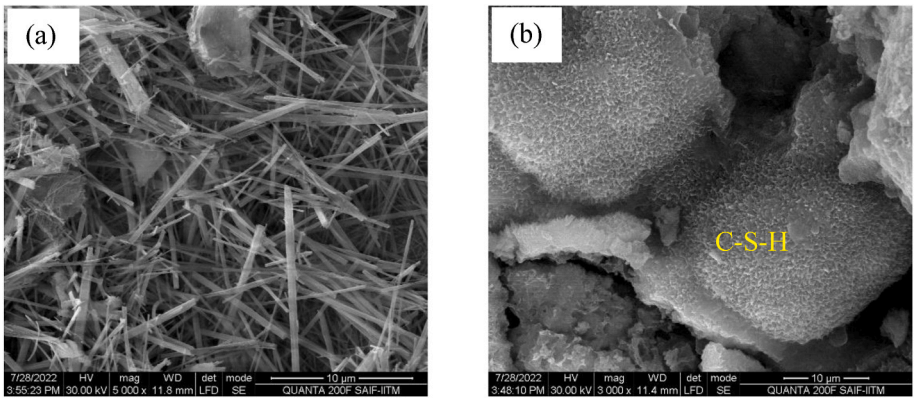

Fig. 10. SEM image of PC-CSA(LY) interface (below neutralisation depth) showing: (a) Ettringite, and (b) C–S–H.

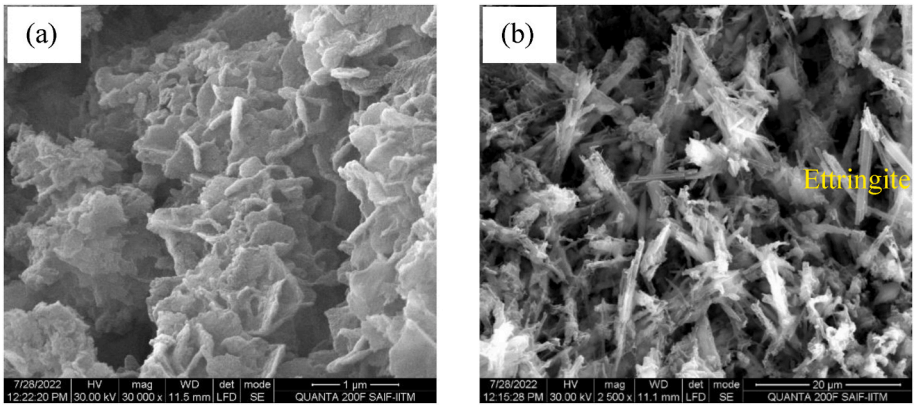

Fig. 11. SEM image of (a) CSA(HY) interface (at neutralisation depth) and (b) Ettringite at interface.

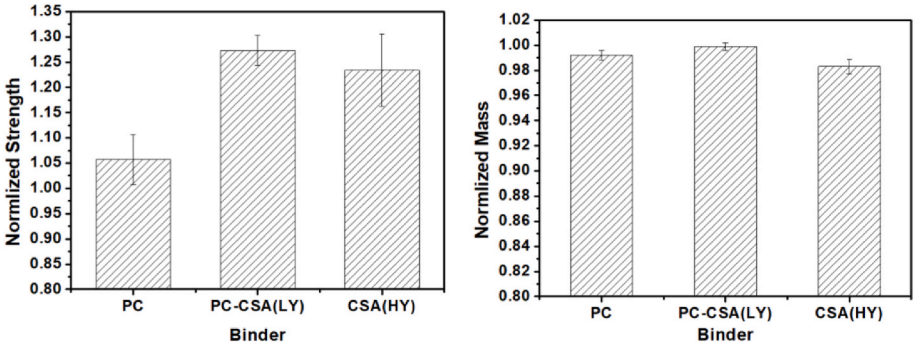

Fig. 12. Normalized strength and normalized mass of exposed specimens from *Location A*.

Surface was rubbed using grit paper to obtain the powder. The powder to represent core was obtained by crushing. The fine powder was sieved in both cases and mixed with distilled water (0.25 g in 10 ml) and stirred for 0.5 h in a test tube rotator. Subsequently, the pH was measured using the pH electrode of autotitrator immediately as well as after 24 h; in both cases measuring similar values. The surface and core pH values are plotted in Fig. 7. The surface pH showed overestimated values due to unavoidable deeper scrubbing. This is stated because the surface didn't give pink colour on phenolphthalein spray, and hence the pH should be less than 9, the phenolphthalein end point. As the scrubbing was uniform, these values can be used to compare the binders. The ratio of surface and core pH for PC, PC-CSA(LY), and CSA(HY) binders was 0.97, 0.97, and 0.93, respectively.

The neutralisation depth was found out by image analysis of the phenolphthalein sprayed specimens in Fig. 6 (d, e, and f). The neutralisation depth of various binders is plotted in Fig. 8. The neutralisation depth of CSA(HY) cement was slightly higher than PC mortar. The higher w/c of 0.45 in CSA(HY) cement with respect to 0.4 in PC to satisfy uniform consistency might have resulted in higher porosity. As a result, the propagation of carbonation front is expected to be faster in case of CSA(HY) binder. In an earlier study, the rate of carbonation in CSA binder was found to be higher than in PC [44]. Furthermore, a low pore solution pH of CSA(HY) cement could be the reason for higher pH reduction after exposure. When the pH is reduced to less than 8.5–10, the CSA cement paste containing ettringite converts into calcite, gypsum, and aluminium hydroxide [45–47].

The morphology of reaction products was analysed below neutralisation depth (at the interface of neutralised and core region) by SEM. Fig. 9 shows the honeycomb like C–S–H and apparently columnar stacking of portlandite in case of PC mortar, supporting an earlier study

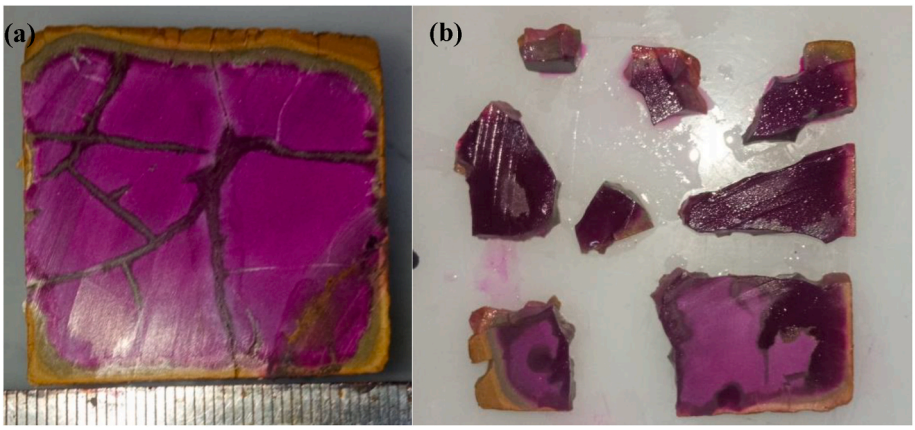

Fig. 13. (a) Zonation in exposed PC treated with phenolphthalein, and (b) Specimens collapsed on slicing.

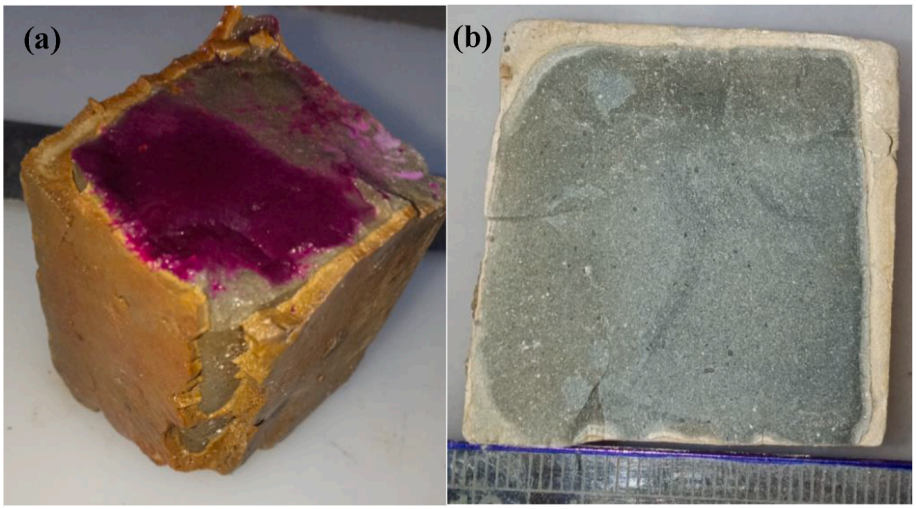

Fig. 14. (a) Zonation observed in exposed PC-CSA(LY) treated with phenolphthalein, and (b) Deteriorated layer as seen in dry state.

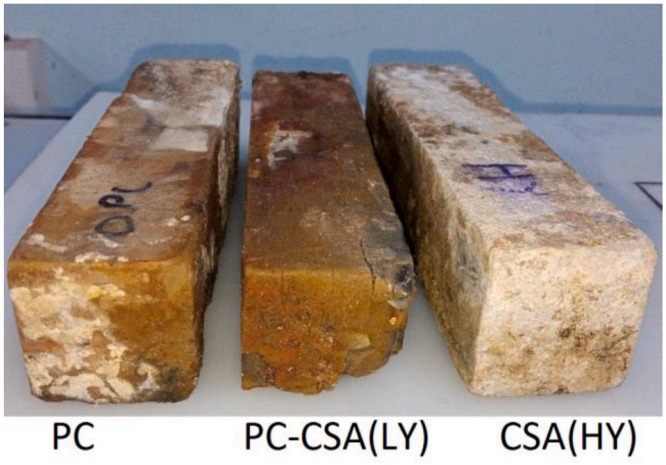

Fig. 15. Specimens exposed at *Location B* – from left: PC, PC-CSA(LY), and CSA(HY).

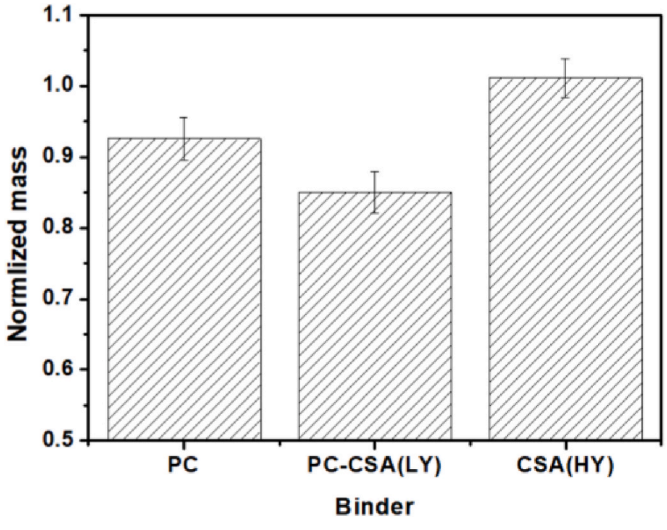

Fig. 16. Normalized mass of exposed specimens with respect to 28-day cured paste.

[48]. The phases were not affected beyond the carbonation front.

Fig. 10 shows the ettringite and C–S–H phases near the interface in PC-CSA(LY) binder. The ettringite needles were formed from the ye'elimite-anhydrite reaction in PC-CSA(LY) binder. These ettringite needles at the interface of CSA(HY) cement are shown in Fig. 11. The surface pH value, visual appearance, and low neutralised depth with the phases preserved below it indicate that the specimens did not reach Stage 3 of the biogenic acid attack. Further, as seen in the upcoming section 3.3,

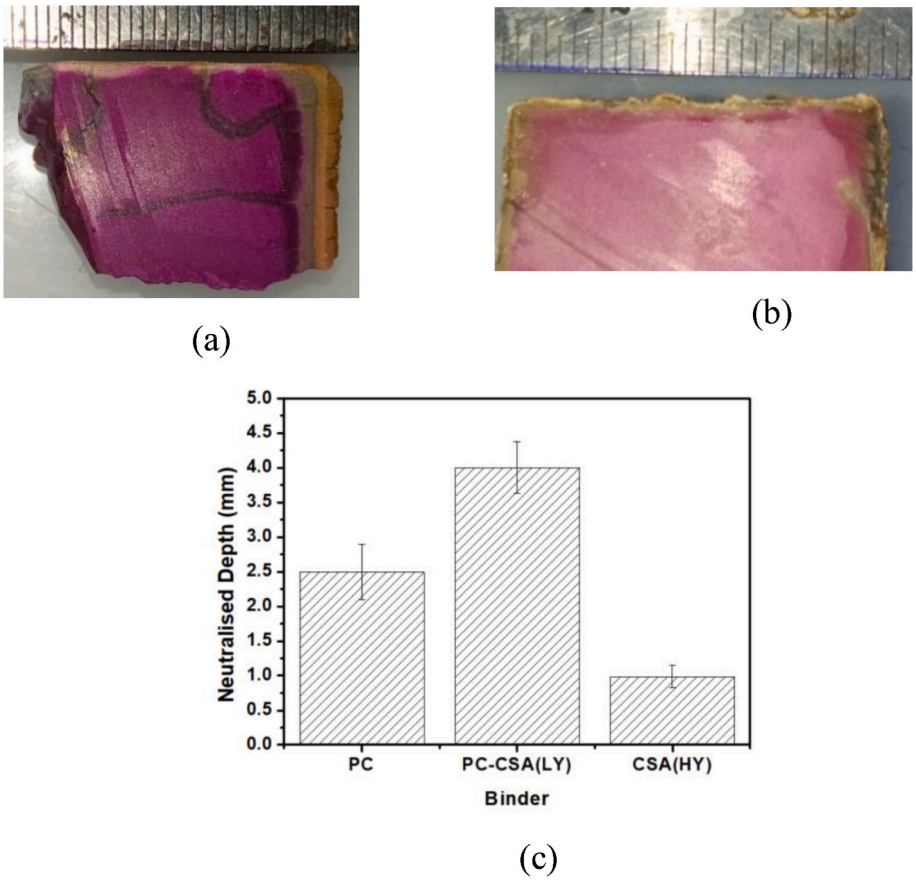

Fig. 17. (a) Phenolphthalein sprayed exposed PC, (b) Phenolphthalein sprayed exposed CSA(HY), and (c) Phenolphthalein assessed neutralisation depth of the binders.

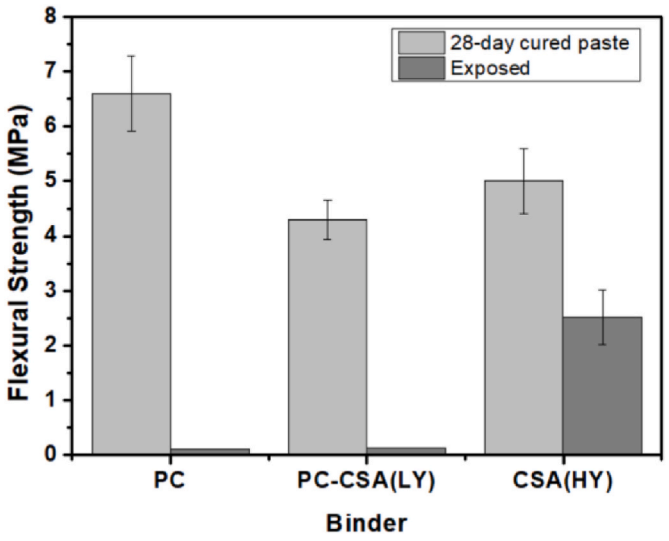

Fig. 18. Flexural strength of 28 day cured and 1-year sewer-exposed paste (w/c = 0.4).

the attached biofilm indicated the specimens were in Stage 2, considering the surface pH values in Fig. 6 are overestimated. The pH reduction is expected to be fast in case of CSA(HY) cement during the carbonation in Stage 1 because of its low porewater pH.

As the specimens were in Stage 2 of biogenic acid attack, the physical properties of binders didn't get affected. The compressive strength of exposed specimens was higher than 28-day cured specimens. The increment could be attributed to sustained hydration during this period and the pore refinement due to carbonation. The carbonation-induced products can precipitate into pores, leading to densification of microstructure [45]. The normalized mass and strength were calculated with respect to 28-day data as shown in Fig. 12. The mass was determined after removing the biofilm. The three binders had statistically similar mass. The normalized compressive strength of CSA(HY) binder was slightly higher than PC after one year exposure, though the 28-day strength had a converse trend as seen in Table 4. Geochemical modelling has revealed that the long term curing of CSA cement produces more monosulfate and strätlingite, resulting in further protection of the ettringite from CO_2 attack [45]. Even though the neutralisation depth due to carbonation for CSA(HY) binder was higher than PC, the physico-mechanical properties were comparable, and thereby, acid resistance could not be differentiated.

3.2.2. *Location B (Stage 3 of biogenic acid attack)*

The paste specimens were taken out of the sewer *Location B* after one year of exposure. The exposed specimens had evidence of attack in the form of clear zonation and cracks, particularly in PC-dominated binders. From Figs. 13 and 14, it is clear that the acid attack environment was so severe that PC-dominated binders were in the Stage 3 of acid attack. This finding was not made based on the pH of concrete surface, as explained in Fig. 1. Surface pH measurement at field may not be accurate because of possible dilution or washing away of acid due to environmental factors. Severe damage and zonation seem to be manifestations of Stage 3 acid attack. Also, it is evident that the PC-dominated binders had characteristic yellow degraded zone, especially visible in Fig. 14. This was possibly the transformed cement paste through biogenic acid attack

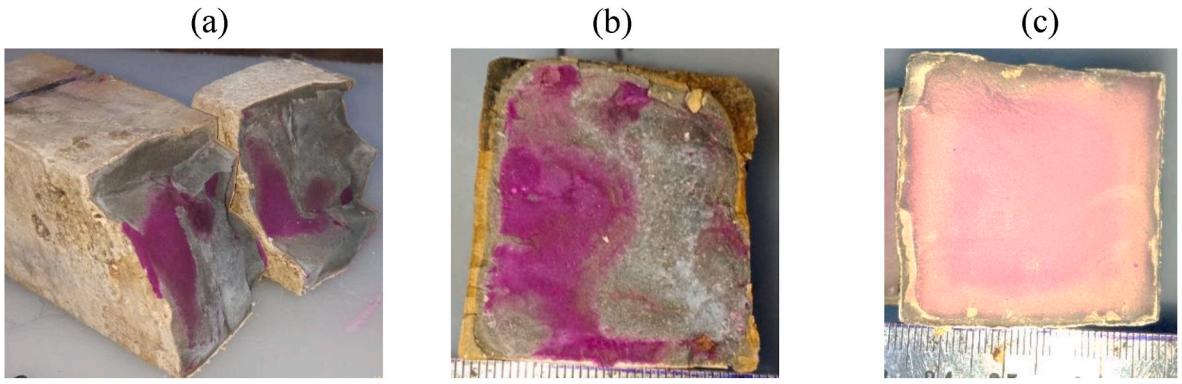

Fig. 19. Phenolphthalein sprayed specimens after flexural strength test: (a) PC, (b) PC-CSA(LY), and (c) CSA(HY).

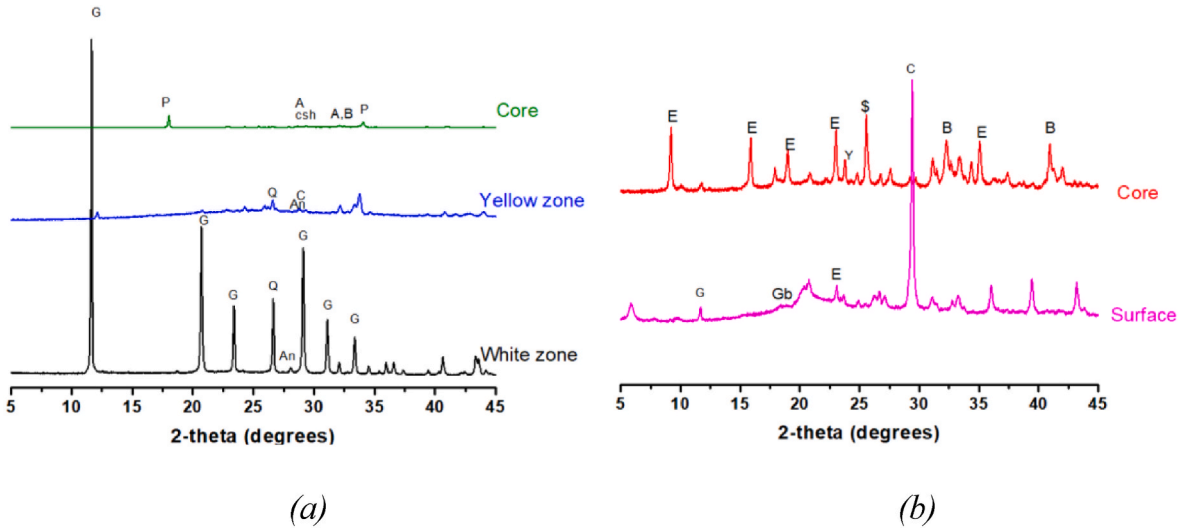

Fig. 20. XRD of various zones of (a) PC paste and (b) CSA(HY) paste exposed in Location B
[G – Gypsum, C – Calcite, An – Anorthite ($Ca(Al_2Si_2O_8)$), E – Ettringite, Y – Ye'elimite, B – Belite, $ – Anhydrite, Q – Quartz, P – Portlandite, A – Alite, Gb – Gibbsite].

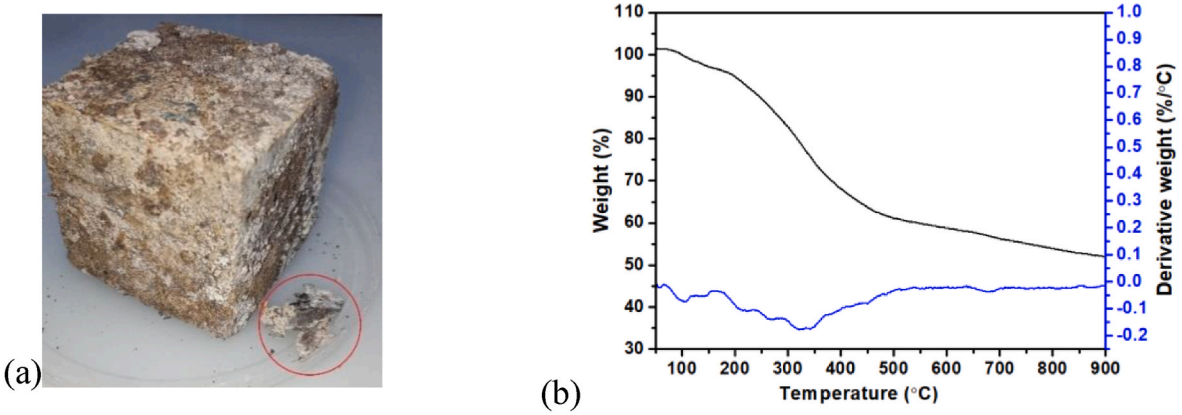

Fig. 21. (a) PC-CSA blend exposed in *Location A* with organic material, and (b) TGA-DTG of slime layer over PC-CSA blend.

and was prone to spalling. Below the yellow degraded zone, relatively intact but neutralised zone of low pH was also visible. Although PC-dominated binders had a reasonably fair core region, they had cracks propagating from periphery of the specimen through degraded and neutralised regions.

As the specimens were severely deteriorated, the relative resistance of the binders could be easily assessed by visual examination (Fig. 15). CSA(HY) specimen appeared to be least affected with respect to size and shape. PC and PC-CSA(LY) specimens had spalled-off regions with the cracks in different regions. Kiliswa et al. [35] also observed higher microcracks in PC concrete than CAC concrete. There, CAC specimens were found to have better integrity than PC specimens after the attack.

Further, the specimens were evaluated based on the mass of deteriorated specimen normalized with that of 28-day cured control specimen, as shown in Fig. 16. The mass loss observed in PC-dominated binders could be attributed to the spalling of the yellow degraded zone after

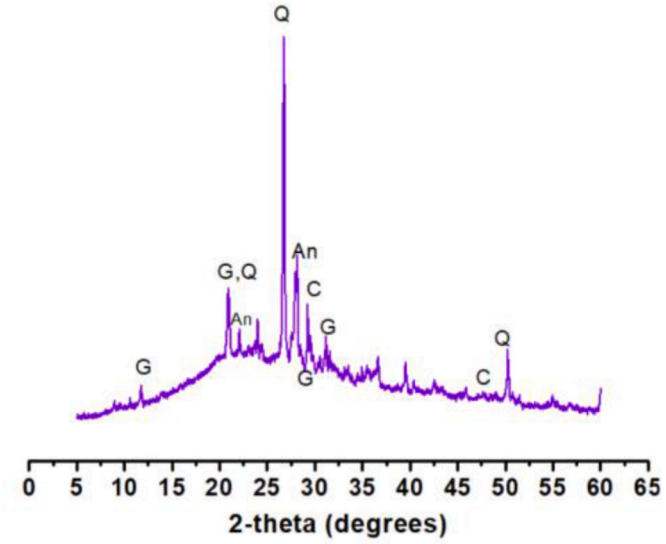

Fig. 22. XRD of slime layer (biofilm) over PC-CSA blend mortar (*Location A*) [G – Gypsum, Q – Quartz, C – Calcite, An – Anorthite ($Ca(Al_2Si_2O_8)$)].

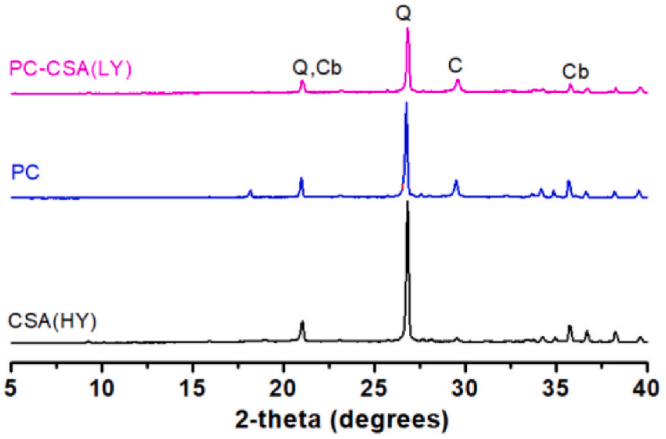

Fig. 23. XRD of ground mortar surface *(from Location A)* after removing biofilm
[Q – Quartz, C – Calcite, Cb – Cristobalite].

biogenic acid attack. The mass loss indicates that nearly 10 % of the PC material was weathered across a period of one year. The residual 90 % mass is inclusive of transformed yellow region ready to spall off. The absence of mass loss in CSA(HY) binder could be attributed to the absence of vulnerable degraded layer. Rather, CSA(HY) binder is characterised by the presence of carbonation and acid attack products filled pores on specimen surface.

The neutralisation depths of the specimens determined by phenolphthalein spraying and image analysis are plotted in Fig. 17. A small colourless region was observed after phenolphthalein spraying on CSA (HY) as well (Fig. 17). The outer yellow zone was absent here, rather a cream coloured intact film was present containing organic material and other products of carbonation and acid attack. In fact, the layer was thin showing the absence of intensive acid attack due to some underlying phenomenon. The lower neutralisation depth observed in CSA(HY), as seen in Fig. 17 (c), could be attributed to the fact that the reaction products filled surface in CSA(HY) could ultimately prevent carbon dioxide ingress also. Otherwise, owing to its lower pore solution pH, the neutralisation depth of CSA(HY) should have been higher due to carbonation, as reported in Ref. [44]. Based on mass loss and neutralised depth, the acid resistance of the binders followed the order: CSA(HY) > PC > PC-CSA(LY). Relatively poor performance of PC is surprising as PC had higher strength than CSA(HY) binder before exposure at 28 days. This points to the inadequacy of strength to predict the durability performance in sewer environment. The material loss in PC specimens, vulnerability of PC against biogenic acid, and superior performance of CSA(HY) highlight intrinsic mechanism in biogenic acid environment.

Flexural strength of specimens is plotted in Fig. 18. There was a severe strength loss in PC-dominated binders (i.e., PC and PC-CSA(LY)). This could be attributed to the weak zones created through the biogenic acid attack. As observed in the literature, this was due to the precipitation of acid attack products such as gypsum and expansive ettringite that induce cracks [49,50]. Additionally, it is known that portlandite will be converted into calcium sulfate, and C–S–H into calcium sulfate and silica gel through biogenic acid attack. The silica gel shrinks considerably on drying and can cause cracking [51]. Further, the specimens tested for flexural strength were sprayed with phenolphthalein (Fig. 19). PC-dominated binders had random regions of pink colour and the non-pink zones could be attributed to the weak zones. CSA(HY) binder had a zone of failure with uniform pink core region. In fact, CSA (HY) cement had the minimum strength loss after field exposure. Even though CSA(HY) binder had slightly lower strength before exposure, the strength loss was lower than PC. This highlights a combination of factors that can favour CSA(HY) binder in biogenic acid attack. It is worth to note that PC-based binders in sewer locations can exhibit catastrophic failure because of the rapid reduction in strength.

3.3. Factors contributing to high acid resistance of CSA(HY) cement

Biogenic acid attack can be considered as an active degradation process, where sustained corrosion is caused by the continuously produced acid by the bacteria [5]. It was observed in Refs. [46,52] that the presence of AH_3[1] phase in CSA(HY) provided increased acid resistance at low pH. As *Thiobacilli* requires extreme acidic environment for its survival, it creates a severe acidic environment, in turn causing rapid corrosion of PC-based binders as can be observed in low pH (pH 0.5) attack [52]. It was observed that CSA(HY) binder outperformed PC in Location B. This was explored by examining the exposed surfaces. The XRD patterns of various zones of biogenic acid attacked specimens of PC and CSA(HY) are shown in Fig. 20.

In Fig. 20(a), XRD patterns of the three visible zones of PC paste: the core region giving pink colour on phenolphthalein test, the yellow region with cracks, and the white region on the surface of the specimen are shown. The white region in PC specimen was mainly gypsum. The underlying yellow layer contained mainly quartz and anorthite along with other phases; traces of these phases could be detected in the XRD pattern for white region. The core region was unaffected, showing the presence of portlandite peaks. XRD patterns for two visible zones in sewer exposed CSA(HY) paste are shown in Fig. 20(b). In contrast to PC, the surface of CSA(HY) binder had less gypsum formation and more calcite precipitation. This indicates lesser susceptibility of CSA(HY) binder. Hence, the core region was pristine, and all hydrated phases of CSA(HY) could be detected.

The two reasons for the overall better performance of CSA(HY) binder will be explained in this section. A biofilm and the underlying altered surface were investigated through advanced characterisation techniques such as TGA, XRD, and SEM. The extent of gypsum formation was further validated by sulfate quantification through turbidimetric technique. The results from *Location A* are discussed in upcoming subsections.

3.3.1. Nature of biofilm

The suspended specimens recovered from both sewer locations had

[1] (cement chemistry notation: C═CaO; A = Al_2O_3; S═SiO_2; $\hat{S}$ = SO_3; F═Fe_2O_3; H═H_2O).

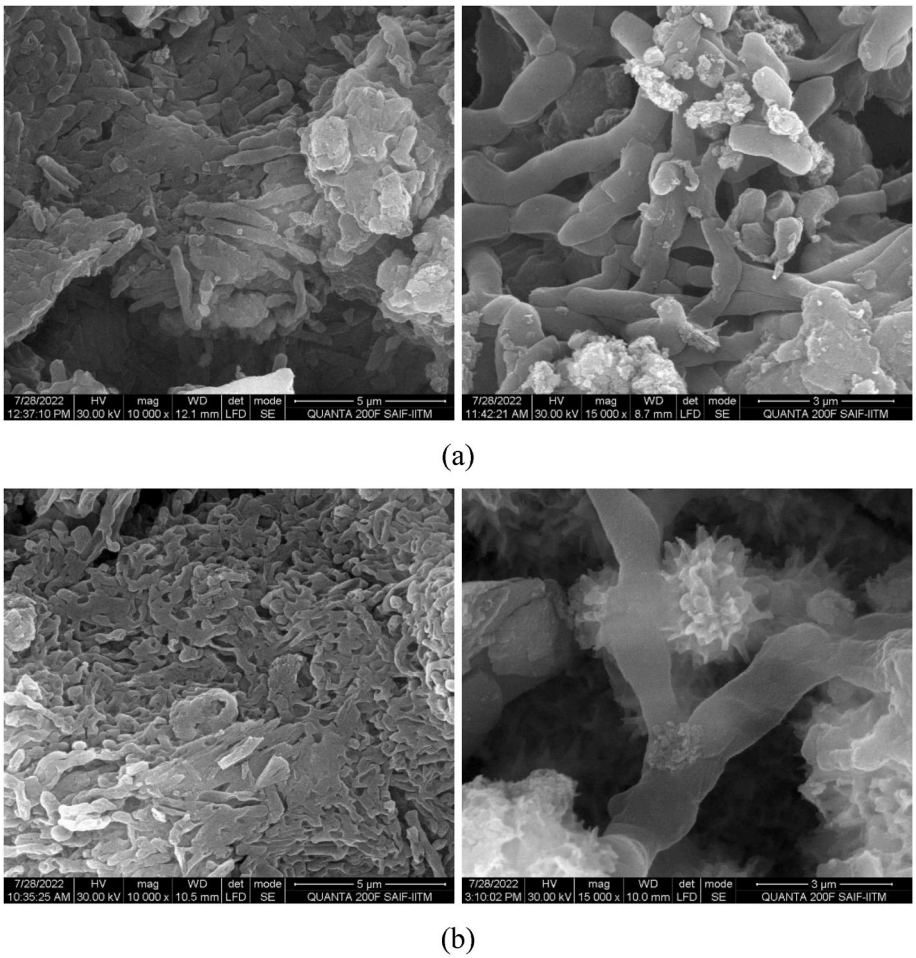

Fig. 24. SEM of sewer exposed specimen surface: bacterial cells in biofilm in (a) hydrated PC mortar (b) hydrated PC-CSA(LY) mortar.

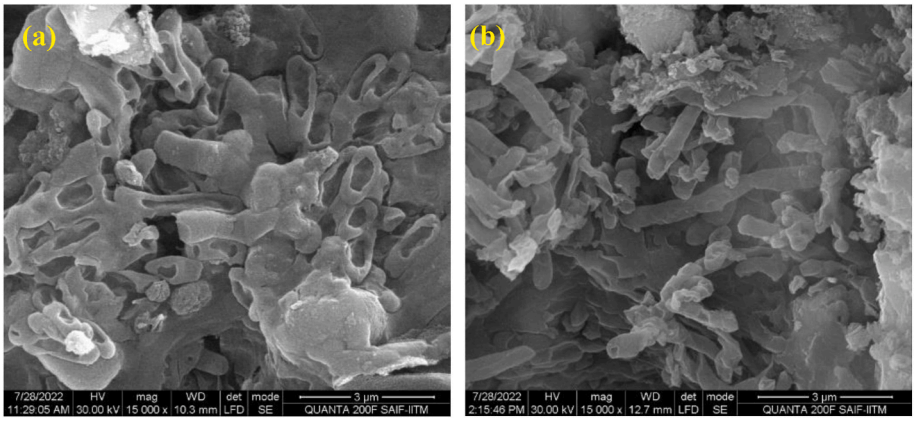

Fig. 25. SEM of (a) Collapsed bacterial cells in hydrated CSA(HY) cement, and (b) Unaffected bacterial cells in hydrated PC.

slime layer/organic material on it (Fig. 21 (a)). This was characterized by TGA, as shown in Fig. 21 (b). The DTG curve had a small peak at ~150 °C corresponding to gypsum. Notably, there was a characteristic wide DTG peak from 200 to 500 °C for the scrapped organic material. This mass loss matched with the DTG peak of biofilm as observed in previous studies [53,54]. The sewer biofilm having thickness around 1 mm is made up of inorganic salts and organic substances such as microbial cells and extracellular polymeric substances containing protein, polysaccharide, and humic material [55].

Further, the biofilm material was taken for XRD analysis and Fig. 22 shows the XRD pattern which is characterized by amorphous hump around 2-theta (2θ) range of 15–40°. This could be attributed to the amorphous content in biofilm: organic substances such as cell biomass and extracellular substances including proteins, humus and polysaccharide, as described earlier. Further, the identified peaks include gypsum, quartz, calcite, and anorthite. The dominant quartz peak can be attributed to the sand grains of mortar. Calcite was formed via carbonation reaction in Stage 1 acid attack and gypsum was formed by biogenic sulfuric acid attack. As PC-CSA(LY) is a system containing AH_3 and C–S–H together, presence of a aluminosilicate phase such as

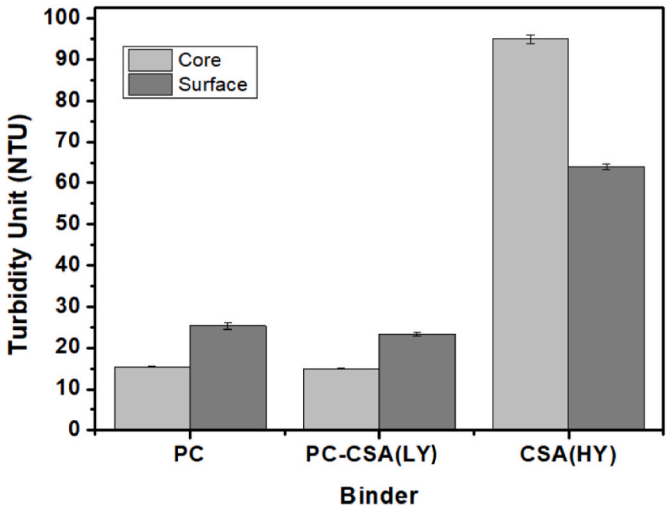

Fig. 26. Relative sulfate content measurement by turbidimetry.

polymerised silica-alumina is possible [45].

The presence of biofilm indicates that specimen had reached the Stage 2 of acid attack at *Location A*. Further, the presence of gypsum in PC-CSA blend indicates that it is either the end of Stage 2 or the beginning of Stage 3 acid attack.

For characterising the material alteration, XRD was performed on the biofilm which was gently removed after scrubbing specimen surface as shown in Fig. 22. Later, XRD was performed on the surface devoid of biofilm and plotted in Fig. 23. Gypsum peaks were not visible in the diffractograms (Fig. 23). The XRD diffractograms didn't have any amorphous hump either, as the surface was devoid of biofilm. This concludes that gypsum formed by biogenic acid did not adhere to the specimen surface, and hence, did not provide any barrier action. Instead, gypsum became part of the biofilm, providing a habitat of bacteria. A similar explanation was reported in Refs. [35,56]. After biogenic acid attack of PC paste, a soft pulpy non-cohesive layer of gypsum was formed [35]. This layer was acidic enough to attack the concrete surface below it [12]. This layer has ideal conditions such as high humidity for protecting the bacteria from dry conditions and low pH for the growth of *Thiobacilli.* As the layer is porous, more bacteria penetrate through this and attack the concrete surface. When the layer thickness is large, oxygen availability at concrete surface is low, and hence, brushing accelerate the attack. However, when layer thickness is small, brushing disturbs the existence of bacteria [22,35,56].

In calcium aluminate cement, the aluminate phases degrade through various stages of neutralisation reaction, with the formation of ettringite as intermediate product. The other neutralisation capacity providing phase AH_3 is stable at a pH of 3–4 and has higher neutralisation capacity [35]. However, ettringite is not stable at low pH, and ultimately converts into gypsum. Hence, it can be hypothesized that such a pulpy gypsum layer habitat and advanced Stage 3 acid attack would be delayed due to neutralisation capacity of CAC. In a similar way, biofilm attachment in CSA(HY) binder having AH_3 can be explained. From the differential neutralisation curve obtained from the sulfuric acid titration in Ref. [46], the neutralisation offered by aluminium hydroxide is visible through the peaks around pH 3–4, in case of CSA and CAC binders. While this neutralisation contribution is absent in Portland cement. It should be noted that AH_3 phase decomposes only at pH 3–4, and thus offers acid resistance to CSA(HY) through the neutralisation capacity. In addition to that, the Stage 3 acid attack in PC and CSA(HY) binders can be explained from the chemical immersion tests with pH 0.5 sulfuric acid [57]. At low pH sulfuric acid attack, gypsum does not provide any barrier, leading to the growth of bacteria within gypsum. The bacteria secrete 100 % sulfuric acid by the H_2S oxidation. This gets diluted by the moisture in the sewer, ultimately leading to low pH sulfuric acid attack. Thiobacillus is stable up to pH of 0.5 [9]. The Stage 3 acid attack at *Location B* can be considered to be similar to pH 0.5 sulfuric acid attack where CSA(HY) outperformed PC [52]. In chemical acid attack of PC, its higher weathering of gypsum layer resulted in relatively poor performance of PC. But, in biogenic acid attack, this weathered gypsum layer incorporated into biofilm, supporting bacterial habitat and aggravating the acid attack. This gypsum-incorporated habitat of bacteria leads to more acid production, further increasing the weathering and deterioration.

3.3.2. *Bacteriostatic effect of CSA binder*

The biogenic acid attacked specimens were characterised to have brown timber coloured surface. The exposed specimen surfaces were further characterised by SEM. The surfaces had a large amount of bacterial population in PC-dominated binders as shown in Fig. 24.

The surface of CSA(HY) binder also had bacterial cells (Fig. 25). The bacterial cells were rod shaped structures having a length of 1–3 μm, indicating the typical characteristics of acidophilic *Thiobacilli*. However, the bacterial cells in CSA(HY) binder were found to be in a collapsed state (dead) while the bacterial cells on the PC surface were unaffected without any change in form. This could be attributed to the bactericidal effect of CSA(HY) binder. The collapse of bacterial cells happened because osmotic stability of the cells might be affected by the reaction of aluminum ions from CSA(HY) binder, causing the leakage of cell organelles [58]. Due to the bacteriostatic effect, bacteria present in CSA (HY) binder cannot reproduce or colonise within the biofilm further. Rather, by this novel property of CSA(HY) binder, the source of acid itself is terminated. This bactericidal or bacteriostatic effect of CSA (HY) binder together with the gypsum-based biofilm causing low constant pH sulfuric acid attack could explain the superior performance of CSA(HY) binder.

The sulfate content on the specimen surface can be a measure of biogenic sulfuric acid produced or calcium sulfate itself. In order to assess the extent of biogenic acid production or gypsum formation, turbidimetric technique was adopted. The core and surface powder

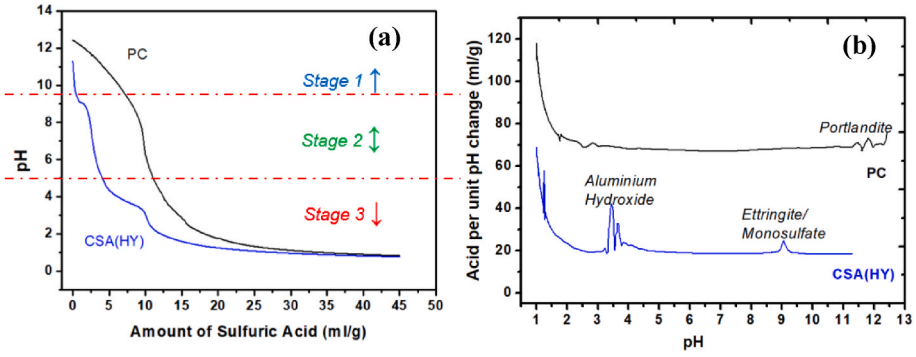

Fig. 27. (a) Powder titration curve, and (b) Differential titration curve for PC and CSA(HY) binder.

suspension were prepared similar to the pH measurement. This was diluted 10 times (1 ml sample in 9 ml distilled water) and 2 ml standard sulfate solution was added into it. A pinch of barium chloride ($BaCl_2$) was added to it for the formation of barium sulfate ($BaSO_4$) from the sulfate in solution. This barium sulfate formation causes the solution to become turbid depending on the concentration. The turbidity of solution was measured after 10 min using a turbidity meter. The measured turbidity in Nephelometric Turbidity Unit (NTU) are plotted in Fig. 26. The higher barium sulfate induced turbidity in CSA(HY) cement indicates the higher sulfate content of these binders. In PC-dominated binders, the sulfate content increased after exposure, whereas it decreased in CSA(HY) binder. This increment in PC-dominated binders could be attributed to bacterial activity in PC, while absence or inefficient bacterial activity in CSA(HY) binder resulted in reduction in sulfate content. This further validates the bacteriostatic effect of CSA(HY) binder.

4. Discussion

Various stages of a biogenic acid attack in sewers can also be simulated using titrimetry. The powder titration curves obtained in Ref. [46] can be utilized for this.

Fig. 27 (a) shows the powder titration curve obtained by conducting titration using 5 % sulfuric acid on hydrated binder powder (<90 μ) suspension (1g in 50 ml distilled water). The various plateaus in Fig. 27 (a) could be understood by switching the axes and differentiating the curve as shown in Fig. 27 (b). As acid is dosed, the pH of suspension decreases gradually. At different pH values, the phases of hydrated binders offer buffering or neutralisation capacity, also evident in form of the peaks (Fig. 27 (b)) corresponding to the plateaus (Fig. 27 (b)). Various stages of biogenic acid attack in Fig. 1 can be superimposed into powder titration curve. The pH range of 9–10 separates Stage 1and Stage 2, and pH range of 4–6 separates Stage 2 and Stage 3 in case of biogenic acid attack. The Stage 3 of biogenic acid attack is characterised by a low pH (<1) sulfuric acid attack inside biofilm. The laboratory chemical acid immersion tests can only simulate the Stage 3 biogenic acid attack. Damion et al. [52] observed the superior acid resistance of CSA(HY), in terms of lower mass loss for CSA(HY) binder, at low pH 0.5 sulfuric acid attack. In the current in-situ biogenic acid attack study, superior performance of CSA(HY) binder was observed. This could be attributed to the neutralisation capacity offered by aluminium hydroxide (AH_3) phase. As seen in Fig. 27 (b), CSA(HY) binder had neutralisation peaks corresponding to AH_3 and ettringite/monosulfate. Whereas PC didn't have the neutralisation contribution from these phases making its acid resistance poorer at severe acidic environment. Though PC has a large amount of portlandite, its reduced neutralisation capacity is highlighted by small portlandite peak in the differential neutralisation curve.

From the titration curves of Fig. 27 (a), the rapid pH reduction in case of CSA(HY) binder compared to PC is visible till a pH of 4–6. The rapid reduction was due to the low poresolution pH and due to absence of portlandite in CSA(HY) binder. This rapid pH reduction was observed in case of *Location A*, where specimens were in Stage 2. Though the pH reduction was rapid in case of CSA(HY) binder till Stage 2, CSA(HY) outperformed PC in Stage 3, as observed in *Location B*. After one-year sewer exposure, the CSA(HY) binder had significantly higher normalized flexural strength and significantly lower mass loss than PC. This huge difference in the performance of binders could be attributed to the bacteriostatic effect. The Stage 2 is characterised by the presence of biofilm and bacterial colonisation. On closely examining the results from two locations, the bacteriostatic effect dominates after Stage 1 and in the beginning of Stage 2. The neutralisation due to AH_3 phase happens in the Stage 3. Hence, the bacteriostatic effect together with the neutralisation of AH_3 offers superior biogenic acid resistance for CSA(HY) binder.

In this study, relative performance of cementitious binders under biogenic acid attack was assessed. However, the actual performance in the field would depend on both physical and chemical characteristics of mortar/concrete mix used in sewer structures. Further studies are required to assess the performance of field mixtures incorporating different cementitious binders.

5. Conclusions

The study summarizes the findings of a field study related to biogenic acid attack of various cementitious binders. The main conclusions of the study can be summarized as below:

- In Stage 1 of acid attack, rapid pH reduction occurred in CSA(HY) binder as compared to PC-dominated binders. This can be attributed to the lower pH of pore solution in CSA(HY) binder.
- CSA(HY) binder outperformed PC dominated binders after 1 year of field exposure (in *Location B*), possibly due to the following factors:
  - o **Nature of gypsum formation**: The gypsum formed by the biogenic acid attack did not act as a barrier, but further aggravated the attack as it became part of the biofilm. Bacteria in this biofilm creates concentrated acid, causing severe constant pH acid attack similar to low pH sulfuric acid attack. In this case, CSA(HY) binder was found to be better than PC. Also, the neutralisation of AH_3 offers higher acid resistance at this low pH.
  - o **Bacteriostatic effect:** The bacteriostatic effect was identified in CSA(HY) binder. By this characteristic of CSA(HY) binder, the source of acid itself was terminated, leading to enhanced acid resistance.

Declaration of competing interest

The authors declare that they have no known competing financial interests or personal relationships that could have appeared to influence the work reported in this paper.

Data availability

Data will be made available on request.

Acknowledgement

The first author would like to acknowledge the doctoral scholarship received from the Ministry of Education, Gov. of India, and the Post Doctoral Equivalent Fellowship from IIT Madras. All authors would like to acknowledge the resources provided by the Department of Civil Engineering at the Indian Institute of Technology (IIT) Madras towards the usage of experimental facilities in this study. The last author is also grateful for the financial support from the New Faculty Seed Grant (CE1920426NFSC008926) by Industrial Consultancy and Sponsored Research (ICSR) centre at IIT Madras. The Centre of Excellence on Technologies for Low Carbon and Lean Construction at IIT Madras is also gratefully acknowledged.

References

[1] W.H. Olmstead, H. Hamlin, Converting portions of the Los Angeles outfall sewer into a septic tank, Eng. News Am. Railw. J. XLIV (1900) 317–318. www.sewerhistory.org/articles/trtmnt/1900_aen18/article.pdf%5CnCached%5Cn.

[2] C. Parker, The corrosion of concrete: 1. The isolation of a species of bacterium associated with the corrosion of concrete exposed to atmospheres containing hydrogen sulphide, Aust. J. Exp. Biol. Med. Sci. 23 (1945) 81–90, https://doi.org/10.1038/icb.1945.13.

[3] C. Parker, The corrosion of concrete: 2. The function of thiobacillus concretivorus (nov. Spec.) in the corrosion of concrete exposed to atmospheres containing hydrogen sulphide, Aust. J. Exp. Biol. Med. Sci. 23 (1945) 91–98, https://doi.org/10.1038/icb.1945.14.

[4] L.A. Allen, The effect of nitro-compounds and some other substances on production of hydrogen sulphide by sulphate-reducing bacteria in sewage, Proc. Soc. Appl. Bacteriol. 12 (1949) 26–38, https://doi.org/10.1111/j.1365-2672.1949.tb03875.x.

[5] M.W. House, W.J. Weiss, Review of microbially induced corrosion and comments on needs related to testing procedures, in: Proc. 4th Int. Conf. Durab. Concr. Struct, vol. 2014, ICDCS, 2014, pp. 94–103, https://doi.org/10.5703/1288284315388.

[6] V. Kaushal, M. Najafi, J. Love, S.R. Qasim, Microbiologically induced deterioration and protection of concrete in municipal sewerage system : technical review, J. Pipeline Syst. Eng. Pract. 11 (2020) 1–10, https://doi.org/10.1061/(ASCE)PS.1949-1204.0000424.

[7] M. O'Connell, C. McNally, M.G. Richardson, Biochemical attack on concrete in wastewater applications: a state of the art review, Cem. Concr. Compos. 32 (2010) 479–485, https://doi.org/10.1016/j.cemconcomp.2010.05.001.

[8] B.R.L. Islander, J.S. Devinny, A. Member, F. Mansfeld, A. Postyn, H. Shih, Microbial e c o l o g y o f c r o w n corrosion in sewers 117 (1992) 751–770.

[9] ASTM C 1894, Standard Guide for Microbially Induced Corrosion of Concrete Products, 2019, pp. 1–8, https://doi.org/10.1520/C1894-19.

[10] A.P. Joseph, J. Keller, H. Bustamante, P.L. Bond, Surface neutralization and H2S oxidation at early stages of sewer corrosion: influence of temperature, relative humidity and H2S concentration, Water Res. 46 (2012) 4235–4245, https://doi.org/10.1016/j.watres.2012.05.011.

[11] A.R. Erbektas, O.B. Isgor, W.J. Weiss, Comparison of chemical and biogenic acid attack on concrete, ACI Mater. J. (2020) 255–264, https://doi.org/10.14359/51720293.

[12] M.G. Alexander, C. Fourie, Performance of sewer pipe concrete mixtures with portland and calcium aluminate cements subject to mineral and biogenic acid attack, Mater. Struct. Constr. 44 (2011) 313–330, https://doi.org/10.1617/s11527-010-9629-1.

[13] L. Ding, W.J. Weiss, E.R. Blatchley, Effects of concrete composition on resistance to microbially induced corrosion, J. Environ. Eng. 143 (2017) 1–9, https://doi.org/10.1061/(ASCE)EE.1943-7870.0001197.

[14] X. Hou, K.A. Steiner, J. Fraczek, J.A. Mahaney, Biogenic Sulfuric Acid Attack and Case Studies, 2020, pp. 33–38.

[15] M.G.D. Gutiérrez-Padilla, A. Bielefeldt, S. Ovtchinnikov, M. Hernandez, J. Silverstein, Biogenic sulfuric acid attack on different types of commercially produced concrete sewer pipes, Cement Concr. Res. 40 (2010) 293–301, https://doi.org/10.1016/j.cemconres.2009.10.002.

[16] C. Magniont, M. Coutand, A. Bertron, X. Cameleyre, C. Lafforgue, S. Beaufort, G. Escadeillas, A new test method to assess the bacterial deterioration of cementitious materials, Cement Concr. Res. 41 (2011) 429–438, https://doi.org/10.1016/j.cemconres.2011.01.014.

[17] M. Peyre Lavigne, A. Bertron, L. Auer, G. Hernandez-Raquet, J.N. Foussard, G. Escadeillas, A. Cockx, E. Paul, An innovative approach to reproduce the biodeterioration of industrial cementitious products in a sewer environment. Part I: test design, Cement Concr. Res. 73 (2015) 246–256, https://doi.org/10.1016/j.cemconres.2014.10.025.

[18] N. De Belie, J. Monteny, A. Beeldens, E. Vincke, D. Van Gemert, W. Verstraete, Experimental research and prediction of the effect of chemical and biogenic sulfuric acid on different types of commercially produced concrete sewer pipes, Cement Concr. Res. 34 (2004) 2223–2236, https://doi.org/10.1016/j.cemconres.2004.02.015.

[19] S. Madraszewski, F. Dehn, J. Gerlach, D. Stephan, Experimentally driven evaluation methods of concrete sewers biodeterioration on laboratory-scale: a critical review, Construct. Build. Mater. 320 (2022), 126236, https://doi.org/10.1016/j.conbuildmat.2021.126236.

[20] L. Wu, G. Huang, W.V. Liu, Methods to evaluate resistance of cement-based materials against microbially induced corrosion: a state-of-the-art review, Cem. Concr. Compos. 123 (2021), 104208, https://doi.org/10.1016/j.cemconcomp.2021.104208.

[21] T. Wells, R.E. Melchers, Modelling concrete deterioration in sewers using theory and field observations, Cement Concr. Res. 77 (2015) 82–96, https://doi.org/10.1016/j.cemconres.2015.07.003.

[22] J. Monteny, E. Vincke, A. Beeldens, N. De Belie, L. Taerwe, D. Van Gemert, W. Verstraete, Chemical, microbiological, and in situ test methods for biogenic sulfuric acid corrosion of concrete, Cem, Concr. Res. 30 (2000) 623–634, https://doi.org/10.1016/S0008-8846(00)00219-2.

[23] A. Bielefeldt, M.G.D. Gutierrez-Padilla, S. Ovtchinnikov, J. Silverstein, M. Hernandez, Bacterial kinetics of sulfur oxidizing bacteria and their biodeterioration rates of concrete sewer pipe samples, J. Environ. Eng. 136 (2010) 731–738, https://doi.org/10.1061/(asce)ee.1943-7870.0000215.

[24] T. Wells, R.E. Melchers, An observation-based model for corrosion of concrete sewers under aggressive conditions, Cement Concr. Res. 61–62 (2014) 1–10, https://doi.org/10.1016/j.cemconres.2014.03.013.

[25] M. Wu, T. Wang, K. Wu, L. Kan, Microbiologically induced corrosion of concrete in sewer structures: a review of the mechanisms and phenomena, Construct. Build. Mater. 239 (2020), 117813, https://doi.org/10.1016/j.conbuildmat.2019.117813.

[26] X. Kang, H. Ye, Antimicrobial alkali-activated slag through self-intercalation of benzoate in layered double hydroxides, Cem. Concr, Composer 130 (2022), 104533, https://doi.org/10.1016/j.cemconcomp.2022.104533.

[27] X. Kang, H. Ye, Antimicrobial performance and biodeterioration mechanisms of alkali-activated slag, Cement Concr. Res. 158 (2022), 106844, https://doi.org/10.1016/j.cemconres.2022.106844.

[28] T. Noeiaghaei, A. Mukherjee, N. Dhami, S.R. Chae, Biogenic deterioration of concrete and its mitigation technologies, Construct. Build. Mater. 149 (2017) 575–586, https://doi.org/10.1016/j.conbuildmat.2017.05.144.

[29] J. Herisson, E.D. van Hullebusch, M. Moletta-Denat, P. Taquet, T. Chaussadent, Toward an accelerated biodeterioration test to understand the behavior of Portland and calcium aluminate cementitious materials in sewer networks, Int. Biodeterior. Biodegrad. 84 (2013) 236–243, https://doi.org/10.1016/j.ibiod.2012.03.007.

[30] C. Grengg, F. Mittermayr, N. Ukrainczyk, G. Koraimann, S. Kienesberger, M. Dietzel, Advances in concrete materials for sewer systems affected by microbial induced concrete corrosion: a review, Water Res. 134 (2018) 341–352, https://doi.org/10.1016/j.watres.2018.01.043.

[31] C. Grengg, N. Ukrainczyk, G. Koraimann, B. Mueller, M. Dietzel, F. Mittermayr, Long-term in situ performance of geopolymer, calcium aluminate and Portland cement-based materials exposed to microbially induced acid corrosion, Cement Concr. Res. 131 (2020), 106034, https://doi.org/10.1016/j.cemconres.2020.106034.

[32] F. Saucier, S. Lamberet, Calcium aluminate concrete for sewers : going from qualitative to quantitative evidence of performance, in: Concr. Aggress. Aqueous Environ. Performance, Test. Model., 2009, pp. 398–407.

[33] A. Buvignier, M. Peyre-Lavigne, O. Robin, M. Bounouba, C. Patapy, A. Bertron, E. Paul, Influence of dissolved-aluminum concentration on sulfur-oxidizing bacterial activity in the biodeterioration of concrete, Appl. Environ. Microbiol. 85 (2019), https://doi.org/10.1128/AEM.00302-19.

[34] A. Buvignier, C. Patapy, M.P. Lavigne, E. Paul, A. Bertron, Resistance to biodeterioration of aluminium-rich binders in sewer network environment: study of the possible bacteriostatic effect and role of phase reactivity, Cement Concr. Res. 123 (2019), 105785, https://doi.org/10.1016/j.cemconres.2019.105785.

[35] M.W. Kiliswa, K.L. Scrivener, M.G. Alexander, The corrosion rate and microstructure of Portland cement and calcium aluminate cement-based concrete mixtures in outfall sewers: a comparative study, Cement Concr. Res. 124 (2019), 105818, https://doi.org/10.1016/j.cemconres.2019.105818.

[36] B.S. Ehrich, L. Helard, R. Letourneux, J. Willocq, E. Bock, Biogenic and chemical sulfuric acid corrosion of mortars, J. Mater. Civ. Eng. 11 (1999) 340–344.

[37] M.F. Zawrah, A.B. Shehata, E.A. Kishar, R.N. Yamani, Synthesis, hydration and sintering of calcium aluminate nanopowder for advanced applications, Compt. Rendus Chem. 14 (2011) 611–618, https://doi.org/10.1016/j.crci.2010.11.004.

[38] G. Valenti, L. Santoro, R. Garofano, High-temperature synthesis of calcium sulphoaluminate from phosphogypsum, Thermochim. Acta 113 (1987) 269–275, https://doi.org/10.1016/0040-6031(87)88330-2.

[39] A.T. Bakera, M.G. Alexander, Sewer concrete subjected to biogenic acid corrosion: analysis of concrete deterioration phases using QEMSCAN, in: MATEC Web Conf. Int. Conf. Concr. Repair, Rehabil. Retrofit., vol. 2022, ICCRRR, 2022, 03012, https://doi.org/10.1051/matecconf/202236403012.

[40] IS 650:1991, Indian Specification for Standard Sand for Testing of Cement, Indian Stand., 1991, pp. 1–11.

[41] G. Jiang, J. Keller, P.L. Bond, Determining the long-term effects of H2S concentration, relative humidity and air temperature on concrete sewer corrosion, Water Res. 65 (2014) 157–169, https://doi.org/10.1016/j.watres.2014.07.026.

[42] ASTM C 1437, Standard Test Method for Flow of Hydraulic Cement Mortar, ASTM Int., 2007, pp. 6–7.

[43] ASTM C348, Standard Test Method for Flexural Strength of Hydraulic-Cement Mortars, Annu. B. ASTM Stand., 2021.

[44] C.W. Hargis, B. Lothenbach, C.J. Müller, F. Winnefeld, Carbonation of calcium sulfoaluminate mortars, Cem. Concr. Compos. 80 (2017) 123–134, https://doi.org/10.1016/j.cemconcomp.2017.03.003.

[45] D. Gastaldi, F. Bertola, F. Canonico, L. Buzzi, S. Mutke, S. Irico, G. Paul, L. Marchese, E. Boccaleri, A chemical/mineralogical investigation of the behavior of sulfoaluminate binders submitted to accelerated carbonation, Cem, Concr. Res. 109 (2018) 30–41, https://doi.org/10.1016/j.cemconres.2018.04.006.

[46] T. Damion, P. Chaunsali, Evaluating acid resistance of portland cement, calcium aluminate cement, and calcium sulfoaluminate based cement using acid neutralisation, Cement Concr. Res. 162 (2022) 1–17, https://doi.org/10.2139/ssrn.4165828.

[47] T. Nishikawa, K. Suzuki, S. Ito, Decomposition of synthesized ettringite by carbonation 22 (1992) 6–14.

[48] W. Franus, R. Panek, M. Wdowin, SEM investigation of microstructures in hydration products of portland cement, Microsc. Microanal. Congr. (2015) 105–112, https://doi.org/10.1007/978-3-319-16919-4.

[49] M. Santhanam, M.D. Cohen, J. Olek, Mechanism of sulfate attack: a fresh look - Part 1; Summary of experimental results, Cement Concr. Res. 32 (2002) 915–921, https://doi.org/10.1016/S0008-8846(02)00724-X.

[50] H.A. Khan, A. Castel, M.S.H. Khan, A.H. Mahmood, Durability of calcium aluminate and sulphate resistant Portland cement based mortars in aggressive sewer environment and sulphuric acid, Cement Concr. Res. 124 (2019), 105852, https://doi.org/10.1016/j.cemconres.2019.105852.

[51] T. Dyer, Influence of cement type on resistance to attack from two carboxylic acids, Cem. Concr. Compos. 83 (2017) 20–35, https://doi.org/10.1016/j.cemconcomp.2017.07.004.

[52] T. Damion, R. Cepuritis, P. Chaunsali, Sulfuric acid and citric acid attack of calcium sulfoaluminate-based binders, Cem. Concr. Compos. 130 (2022), 104524, https://doi.org/10.1016/j.cemconcomp.2022.104524.

[53] Y. Shen, P.C. Huang, C. Huang, P. Sun, G.L. Monroy, W. Wu, J. Lin, R.M. Espinosa-Marzal, S.A. Boppart, W.T. Liu, T.H. Nguyen, Effect of divalent ions and a polyphosphate on composition, structure, and stiffness of simulated drinking water biofilms, Npj Biofilms Microbiomes 4 (2018) 1–9, https://doi.org/10.1038/s41522-018-0058-1.

[54] K.C. Cheng, J.M. Catchmark, A. Demirci, Enhanced production of bacterial cellulose by using a biofilm reactor and its material property analysis, J. Biol. Eng. 3 (2009) 1–10, https://doi.org/10.1186/1754-1611-3-12.

[55] W. Li, T. Zheng, Y. Ma, J. Liu, Current status and future prospects of sewer biofilms: their structure, influencing factors, and substance transformations, Sci. Total Environ. 695 (2019), 133815, https://doi.org/10.1016/j.scitotenv.2019.133815.

[56] M. Alexander, A. Bertron, N. De Belie, Performance of Cement-Based Materials in Aggressive Aqueous Environments, 2013.
[57] T. Damion, Performance of Calcium Sulfoaluminate- Based Binders in Acidic Environments, 2023.
[58] D.H. Nies, Microbial heavy-metal resistance, Appl. Microbiol. Biotechnol. 51 (1999) 730–750, https://doi.org/10.1007/s002530051457.